First principles surface thermodynamics of industrial supported catalysts in working conditions

2008 J. Phys.: Condens. Matter 20 064235

(http://iopscience.iop.org/0953-8984/20/6/064235)

J. Phys.: Condens. Matter **20** (2008) 064235 (11pp) doi:10.1088/0953-8984/20/6/064235

First principles surface thermodynamics of industrial supported catalysts in working conditions

P Raybaud[1,4], D Costa[1,2,5], M Corral Valero[1,3,6], C Arrouvel[1,2], M Digne[1,3,6], P Sautet[3] and H Toulhoat[1]

[1] IFP, 1&4 av. Bois Préau, 92852 Rueil Malmaison Cedex, France
[2] Laboratoire de Réactivité de Surface—UMR 7609 CNRS—Université Pierre et Marie Curie, 4 Place Jussieu, 75252 Paris Cedex 05, France
[3] Université de Lyon, Laboratoire de Chimie, Institut de Chimie de Lyon, Ecole Normale Supérieure de Lyon and CNRS, 46 Allée d'Italie, 69364 Lyon Cedex 07, France

E-mail: pascal.raybaud@ifp.fr

Received 3 September 2007, in final form 6 November 2007
Published 24 January 2008
Online at stacks.iop.org/JPhysCM/20/064235

Abstract

Ever stronger environmental concerns prompt the research in the area of heterogeneous catalysis to play an ever more crucial role to produce ever cleaner fuel from the refining of petroleum effluents. The catalytic active phase is often used in a dispersed state over a porous oxide material. This paper is a review of recent progress brought by periodic density functional theory (DFT) calculations in the area of two relevant industrial supported catalysts. We focus on two important supports used in the refining industry: anatase-TiO_2 and γ-alumina. According to the various reaction conditions, the presence of H_2O, H_2 and H_2S may change the surface states of the support. In particular, it is crucial to know and control the hydroxylation state depending on temperature and partial pressure of reactants (H_2O, H_2, H_2S). The support effects on the catalytic active phases are presented for MoS_2 particles, used in hydrodesulfurization catalysis, and for Pd particles, used in hydrogenation catalysis. It is shown how the wetting property and equilibrium morphology of the active phase depend on the support. A discussion on the impact for catalytic activities is provided.

(Some figures in this article are in colour only in the electronic version)

1. Introduction

In the context of strong environmental concerns, the production of ever cleaner fuels by catalytic chemical processes (such as hydrodesulfurization, hydrocracking, hydrogenation . . .) remains a major concern of the refining industry. The challenges for research in the area of heterogeneous catalysis are to provide highly active and selective catalytic materials for important reactions such as hydrodesulfurization (i.e. removal of sulfur from organic molecules under hydrogen pressure) or selective hydrogenation of diolefins into olefins. These catalytic materials are made of an active phase dispersed over an oxide support. The active phases can be constituted of small particles of transition metals or transition metal sulfides depending on the reacting environment. For hydrodesulfurization (HDS) reactions, the release of H_2S after S removal from the organic molecules implies that the stable active phase is a transition metal sulfide phase. For hydrogenation reactions, the absence of H_2S in the gas phase allows the use of Ni, Pd and Pt transition metals as an active phase. The oxide support widely used in the refining industry is γ-alumina, which is one of the metastable polymorphs of transition aluminas exhibiting high surface areas and interesting acid–base properties [1]. Other oxide supports, such as the anatase-TiO_2 discussed in this paper, are the subject

[4] Authors to whom any correspondence should be addressed.
[5] Present address: Laboratoire de Physicochimie des surfaces—UMR 7045 CNRS—Ecole Nationale Supérieure de Chimie de Paris, 11 rue Pierre et Marie Curie, 75231 Paris cedex, France.
[6] Present address: IFP-Lyon, BP 3-69390 Vernaison, France.

of numerous investigations. Several interesting industrial applications are well known for anatase-TiO_2 nanocrystals: either in dye-sensitized solar cells [2], as photocatalysts [3] or as the support of heterogeneous catalysts [4].

For HDS reactions, the catalyst is a γ-alumina supported 'CoMoS' or 'NiMoS' sulfide. Numerous cutting-edge experimental techniques have been used to better characterize the catalytically active 'CoMoS' or 'NiMoS' phases [5, 6] and the support itself [1]. The active phase is made of MoS_2 sheets with nanometre sizes (less than 30 Å). Each MoS_2 sheet can be regarded as a two dimensional quasi-hexagonal structure, where the Mo plane is sandwiched between two S layers and is 'decorated' by Co or Ni atoms at the edges. The continuous improvement of such complex catalysts requires the capability to take up multiple research issues raised by the properties related to the active phase, to the γ-alumina phase and to the two interacting phases in reaction conditions. Indeed, improvements of the active phase are rarely obtained without a careful consideration of the support either at the preparation steps or in reaction conditions.

First principles modelling has brought numerous insights and concepts on the precise atomistic and electronic properties of transition metal sulfides [7–9] and of the Co(Ni)MoS phase, contributing to new progress in this area [10]. The challenge for first principles modelling was pushed further when it was attempted to address the support effects on the catalytic properties of such complex materials.

In the case of oxide supported metallic active phases, the interaction of the support with the active phases is also known to play an important role in the activity of the final catalysts [11]. The role of the support becomes all the more crucial as the dispersion of the metal such as palladium is high [12]. A review [13] highlighting support effects on the structural and electronic properties of metallic active phases reveals that the behaviour of the metallic phase is sensitive to the support's surface.

Addressing such complex and subtle effects requires an atomistic description of the nature of the interaction between the chemical species (hydroxyl groups, Lewis sites) present at the support surface and the sites of the active phase. If chemical bonds connecting the active phase (either the transition metal sulfide or the metallic phase) and the support exist in reaction conditions, the active phase should not be considered as an isolated phase but rather as a binary phase involving electronic redistribution between the oxide support and the active phase. According to the type of interaction, electronic and geometric effects may affect the intrinsic activity of the sites.

Very few experimental techniques are able to give direct nanoscale insights on the active phase-support interfaces. Regarding first principles calculations, these questions are very challenging. First, relevant surface models of the supports in reaction conditions have to be developed. Then, models for the interacting systems have also to be investigated with great care because the size of the simulated supercell (reaching 300 to 400 atoms in the most relevant cases) pushes the limits of current density functional calculations on high performance computers.

Thanks to the giant step forward provided by the development of density functional theory (DFT) [14, 15] and its elegant implementation in plane wave software such as VASP [16, 17], DACAPO [18], Wien2k [19] and CASTEP [20], modern *first principles* modelling provides a rational way to investigate the local properties of active sites on various catalytic surfaces.

The goal of the present paper is thus to give an overview of relevant achievements obtained by *density functional* modelling of two types of industrial supported catalysts and to illustrate how this modelling can be used to bring new insights on such intricate systems. After a first section devoted to a brief presentation of methodological aspects, we present recent advances provided by DFT modelling of the properties of γ-alumina and anatase-TiO_2 surfaces and their hydroxylation states in relevant working conditions. Then, we show how the nature of the active phase–support interaction was investigated for two relevant industrial catalytic materials. On the one hand, we focus on the comparison of the effects of two important oxide supports for MoS_2 catalysts: γ-alumina and anatase-TiO_2. The impact on the equilibrium morphology of the MoS_2 active phase driven by wetting effects will be stressed. On the other hand, considering γ-alumina supported Pd systems used in hydrogenation reactions, we show how the interaction of the active phase depends on the hydroxylation state of γ-alumina surfaces. The impact on the adsorption of small molecules on a supported Pd_4 cluster is also reported.

2. Theoretical method

The general approach which combines DFT calculations and the chemical potential of the gas phase was previously undertaken to study surface thermochemistry of GaAs [21, 22], c-BN [23] and α-Fe_2O_3 [24]. An interesting overview of *first principles* surface thermodynamics can be found in a recent review [25]. To our knowledge, this approach successfully applied to MoS_2 and Co(Ni)MoS active phase was first reported in [26, 27]. More recent studies have also used this systematic approach to investigate hydroxylated surfaces of complex industrial support such as γ-alumina [28]. This is an elegant way to bridge the gap between DFT calculations (carried out at 0 K) and realistic working conditions.

To determine by theoretical approaches the stable chemical species on the catalytic surface in reaction conditions (p_i, T) at thermodynamic equilibrium, one can minimize the surface energy given by the following general expressions:

$$\Gamma_{hkl}(p_i, T, \theta^i_{hkl}) = \Gamma^0_{hkl} + \sum_i \theta^i_{hkl}(E^i_{\text{ads}} + \Delta\mu_i) \quad (1)$$

$$\Delta\mu_i(T, p_i) = h^0_i - Ts^0_i + RT \ln\left(\frac{p_i}{p^0}\right) - e_i \quad (2)$$

Γ_{hkl} is the surface energy of the surface with *(hkl)* crystallographic orientation. Γ^0_{hkl} is the surface energy of the reference *(hkl)* surface (generally in vacuum or in absence of any adsorbed species). E^i_{ads} is the adsorption energy of molecule i, such as H_2S, H_2O or H_2 in the cases investigated so far. The most stable adsorption mode of molecule i (either dissociative or non-dissociative) is determined as a function of its surface coverage θ^i_{hkl}. The molecule may thus generate

different types of species (M–H_2S, M–H_2, M–H_2O, M–SH, M–OH, MH...) depending on its stable adsorption mode defined by the most exothermic adsorption energy.

$\Delta\mu_i$ is the chemical potential of molecule i in the gas phase: it depends on the partial pressures of H_2S, H_2O or H_2 and temperature according to (2). h_i, s_i and e_i are the enthalpy, entropy and internal energy of the gas phase molecule.

Equations (1) and (2) furnish a direct connection between the chemical state of the catalytic surface and reaction conditions assuming that at equilibrium the stable state of the surface is defined as the one minimizing its surface energy. At this stage, no assumption is made on the methodology used to calculate the energy terms in (1) and (2). When considering chemical processes involving bond breaking and bond formation at a surface, the so-called *ab initio* methods (excluding any empirical fits) are required. The formalism of the density functional theory (DFT) enables the Schrödinger equations to be solved for complex systems with a minimal set of approximations [14, 15]. From a practical point of view, the software implementation of the so-called *first principles* modelling technique furnishes the best compromise between computational resources and system sizes required for realistic simulations.

In the present case, the energy values such as Γ^0_{hkl} and E^i_{ads} are the outcome of simulations based on DFT within the generalized gradient approximation (GGA) [29]. To solve the Kohn–Sham equations, works reported hereafter use the Vienna *Ab Initio* Simulation Package (VASP) [16, 17]. The ion–electron interactions are treated by pseudopotentials such as Vanderbilt ultrasoft pseudopotentials [30, 31] for earlier works reported in this paper, and within the projector augmented wave (PAW) formalism [32] for more recent results. For simulations of solid phases with delocalized electronic charges it is efficient to employ a plane wave basis set to project the wavefunctions in a 3D supercell representing the systems (bulk or slabs) with periodic boundary conditions. All detailed hypotheses of the calculations (such as electronic convergence criteria, energy cut-off, k-point mesh, relaxation conditions...) can be found in papers cited herein.

3. Surface state of the anatase-TiO_2 and γ-alumina supports

Regarding the support effects on the active phase, two aspects must be considered. On the one hand, abundant experimental research has been carried out on the γ-alumina support since the pioneering work of Lippens and de Boer [33], using techniques such as nuclear magnetic resonance (NMR) [34–36], vibrational spectroscopies [37–40], x-ray diffraction (XRD) [1] and transition electron microscopy (TEM) [41]. However, the rational description of the γ-Al_2O_3 bulk structure and the surface species (hydroxyls and acid–base sites...) suffered from ambiguous interpretation due to a lack of atomistic investigation.

To overcome this situation, a systematic DFT determination of γ-alumina and anatase-TiO_2 surfaces was mandatory. The lack of a precise crystallographic structure of γ-alumina meant that preliminary DFT studies first focused on the bulk structure of this support. These studies revealed the existence of non-spinel Al sites in the bulk [42–44].

The subsequent step was the determination of the stable species at the surface of γ-alumina and anatase-TiO_2 in reaction conditions [28, 45–47]. The thermodynamic approach explained in section 2 was successful in determining the surface energy as a function of the various reaction conditions (p_{H_2O}, p_{H_2S}, p_{H_2} and T). Figure 1 reports the surface energies and water coverages for the relevant γ-alumina and anatase-TiO_2 surfaces as a function of p_{H_2O} and T. The water coverage is directly linked with the hydroxylation state and the acid–base properties of the surfaces which are crucial for understanding the catalytic activities and the interaction with the active phase. By definition, the surface hydroxyl concentration is twice the water coverage. The results obtained in the works by Digne *et al* and Arrouvel *et al* [28, 45–47] can be summarized as follows. The surface energies of the anatase-TiO_2(101) and γ-alumina (100) surfaces are lower than those of the anatase-TiO_2(001) and γ-alumina(110). Furthermore, the degree of hydroxylation and nature of hydroxyl groups depend on the crystallographic orientation of the surface and thus on support morphologies. The anatase-TiO_2(101) and γ-alumina (100) surfaces (with the lower surface energies) remain non-hydroxylated in T and p_{H_2O} conditions corresponding to hydrodesulfurization or hydrogenation reactions (represented by the rectangular region in figure 1).

This implies that Lewis sites (uncoordinated Ti or Al sites) are predominant on these two surfaces. In contrast, the anatase-TiO_2(001) and γ-alumina(110) surfaces are hydroxylated. The atomistic structures reported in figures 2 and 3 illustrate the type of sites and hydroxyl groups present on TiO_2(001) and (101) surfaces. Figures 2 and 3 also show that the full dehydration of the (101) surface occurs at a temperature significantly lower (450 K) than for the (001) surface (850 K). As a result, Ti–OH groups are present on the (001) surface in reaction conditions, whereas the (101) surface is fully free from OH species. For γ-alumina, similar diagrams have been constructed, and revealed that at standard pressure of water the dehydration temperature of the (110) is significantly higher (1100 K) than that of the (100) surface (600 K) [28, 45].

On the hydrated surfaces, various types of hydroxyl groups are stabilized at the surface: these groups can be one-, two- or threefold coordinated to Al or Ti atoms. Numerous characterizations by infra-red (IR) spectra of γ-alumina and anatase-TiO_2 are available in the literature [48–50]. However, the precise assignments of the spectra were missing in the absence of any DFT data. In the case of γ-alumina, table 1 gives the calculated OH stretching frequencies compared with the experimental OH bands observed in the IR spectra of anatase-TiO_2 and γ-alumina [50] for different types of hydroxyls. For γ-alumina, the earlier empirical Knözinger's assignment [38] was thus challenged by the DFT results [28, 45]. Furthermore, proton NMR characterization has also revealed that the γ-alumina surface concentration of hydroxyls significantly diminishes from 8.2 OH nm^{-2} at 450 K to 2.1 OH nm^{-2} at 880 K [34], which is also in quantitative agreement with the DFT estimate of OH coverage at equilibrium (figure 1). For anatase-TiO_2, the combination

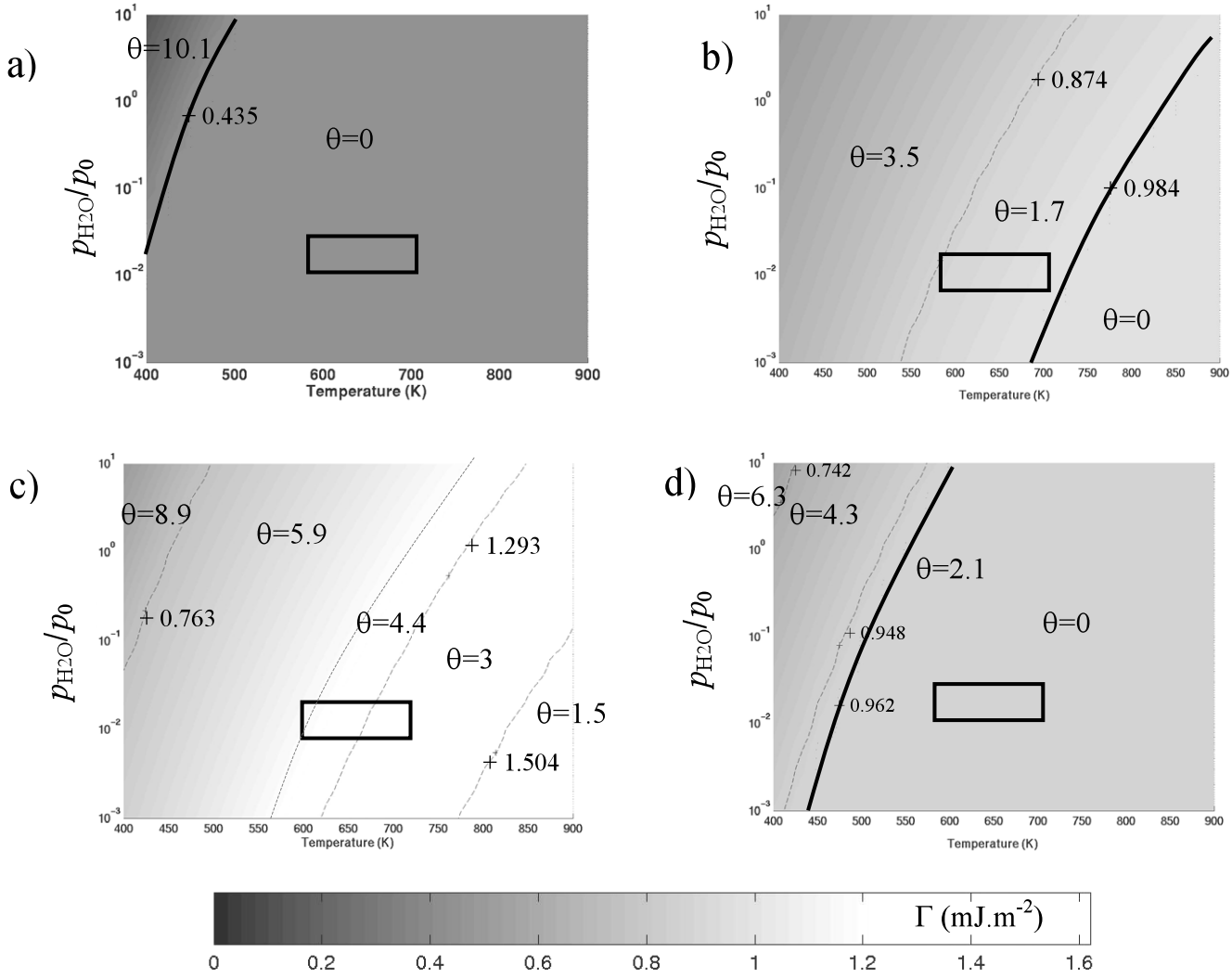

Figure 1. (Γ, P, T) diagrams representing the isovalues of surface energy as a function of T and P_{H_2O} for different surfaces: (a) TiO_2(101) surface, (b) TiO_2(001) surface, (c) γ-Al_2O_3(110) surface, (d) γ-Al_2O_3 (100) surface. Values of water coverages (θ_{hkl}) are also reported on the different domains. Rectangular windows indicate the conditions prevailing in an industrial HDS reaction. (Adapted from [28] and [46].)

of TEM, infra-red (IR) analysis and DFT calculation of the OH frequencies revealed that modifying the morphology of the nano-crystallites of TiO_2 may provide an interesting way to control the acid–base properties of the supports [46, 51]. This comparison between theory and experiment validates the models of the surfaces determined by the DFT atomistic thermodynamics at equilibrium in working conditions, where temperature and non-negligible partial pressures of reactants permit us to rapidly reach the equilibrium at the surface.

For hydrodesulfurization reactions, the effect of partial pressure of H_2S must also be taken into account. Figure 4 shows that this implies that the anatase-TiO_2(001) surface is partially sulfided ($\theta_{001}^{H_2S} = 1.7$ H_2S nm^{-2}). The local structure of the partially sulfided (001) surface is reported in figure 4, where the S atom resulting from the dissociative adsorption of H_2S is in a bridging position between two Ti atoms. This result provides an explanation of x-ray photoelectron spectroscopy (XPS) revealing the core level shift of Ti in a sulfo-reductive environment [52].

Table 1. Calculated vibrational stretching frequencies of γ-alumina surface hydroxyl groups. (Details about OH stretching frequency calculations including anharmonic corrections are given in [28, 45].)

Site	Surface	ω_{calc} (cm^{-1})	ω_{exp} (cm^{-1})
HO-μ_1-Al_{IV}	(110)	3842	3785–3800
HO-μ_1-Al_{VI}	(100)	3777	3760–3780
HO-μ_1-Al_V	(110)	3736	3730–3735
HO-μ_2-Al_V	(110)	3707	3690–3710
HO-μ_3-Al_{VI}	(100)	3589	3590–3650

As a consequence, it is important to consider the correct surface state of the support for investigating the interaction with the active sites as shown in the following sections.

4. Morphology and wetting effects for supported MoS_2 catalysts

As suggested in section 1, many experimental works revealed that support effects cannot be overlooked when investigating

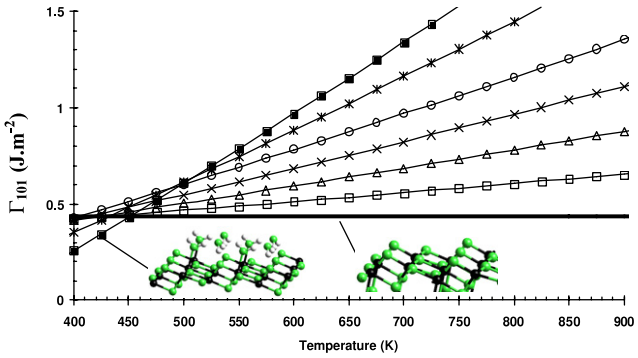

Figure 2. Surface energy of the (101) surface of anatase-TiO_2 as a function of temperature for different coverages of H_2O at $P_{H_2O} = 1$ bar, calculated according to equation (1). Each straight line corresponds to the following water coverage: (——) $\theta_{101} = 0.0$; (□) $\theta_{101} = 1.3$ H_2O nm^{-2}, (Δ) $\theta_{101} = 2.5$; (×) $\theta_{101} = 3.8$; (○) $\theta_{101} = 5.1$; (∗) $\theta_{101} = 7.6$; (■) $\theta_{101} = 10.1$. Reprinted from [46]. Copyright 2004, with permission from Elsevier.

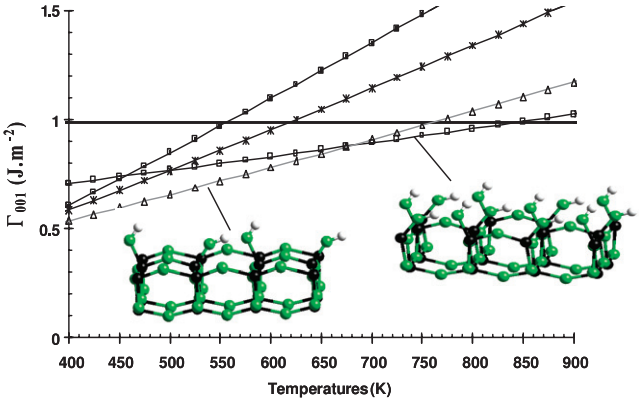

Figure 3. Surface energy of the (001) surface of anatase-TiO_2 as a function of temperature for different coverages of H_2O at $P_{H_2O} = 1$ bar, calculated according to equation (1). Each straight line corresponds to the following water coverage: (——) $\theta_{001} = 0.0$; (□) $\theta_{001}^{H_2O} = 1.7$ H_2O nm^{-2}; (Δ) $\theta_{001}^{H_2O} = 3.5$; (∗) $\theta_{001} = 5.2$; (■) $\theta_{001} = 6.9$. Reprinted from [46]. Copyright 2004, with permission from Elsevier.

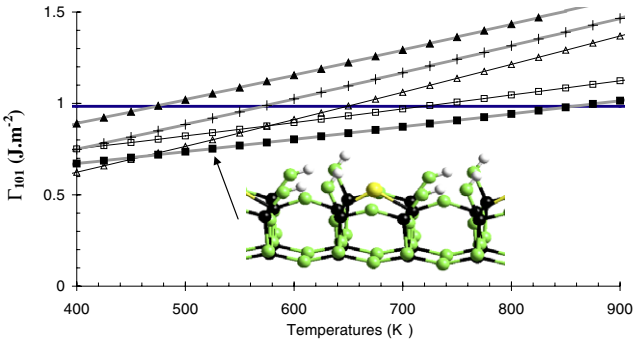

Figure 4. Surface energy of the (001) surface of anatase-TiO_2 as a function of temperature for different coverages of H_2O and H_2S at $P_{H_2O} = 10^{-2}$ bar and $P_{H_2S} = 1$ bar. (——) $\theta_{001} = 0.0$ molecule nm^{-2}; (□) $\theta_{001}^{H_2O} = 1.7$ H_2O nm^{-2}, (Δ) $\theta_{001}^{H_2O} = 3.5$; (■) $\theta_{001}^{H_2S} = 1.7$ H_2S nm^{-2}; (▲) $\theta_{001}^{H_2S} = 3.5$; (+) $\theta_{001}^{H_2O} = 1.7$ and $\theta_{001}^{H_2S} = 1.7$. Reprinted from [47]. Copyright 2004, with permission from Elsevier.

the catalytic properties of the MoS_2 catalysts industrially used for hydrodesulfurization reactions [4, 53]. At an industrial scale, γ-alumina is the preferred support due to its well optimized porous and acidic properties [1]. At a laboratory scale, one well known experimental result is that the anatase-TiO_2 supported MoS_2 catalyst exhibits a higher intrinsic HDS activity than γ-alumina supported MoS_2 [54]. However, due to less optimal porous properties, anatase-TiO_2 is not chosen nowadays for industrial applications.

Numerous proposals were put forward to explain these observations such as electronic effects [54], orientation effects [55] or indirect promotion by Ti [52, 56, 57]. Even if EXAFS data provided some insights on the local distances and coordination at the interface between the active phase and the support [58], it remained very difficult to provide a clear atomistic representation of the active phase–support interface. As a consequence, modern first principles techniques were expected to furnish new concepts related to the subtle effects of active phase–support interaction. Two recent works by Arrouvel *et al* [59] and by Costa *et al* [60] addressed this complex question, and their main results concerning the non-promoted MoS_2 active phase are reported in the following paragraphs.

The first insight was that support effects can only be understood if the stable state (hydroxylation or sulfidation state) of the support's surface reaction conditions is taken into account for the model. Then, a systematic approach based on DFT thermodynamic models of the binary phase TiO_2- and γ-Al_2O_3-supported Mo_6S_n clusters was undertaken, where n varies according to the chemical potential of sulfur fixed by the HDS reaction conditions (T, p_{H_2} and p_{H_2S}). Such Mo_6S_n triangular clusters are models representing the active edge sites, present on the MoS_2 sheets. Each individual MoS_2 sheet of nanometre sizes is a two dimensional (2D) structure where the Mo atomic plane is sandwiched between two S layers. This 2D structure has a deformed hexagonal shape truncated by two types of edges called an 'Mo edge' or 'S edge'. The size of the sheet is defined as the diameter (D) in what follows. The active sites are present on these two edges and interact with molecules or with the support's surface itself. Hence, the triangular Mo_6S_n clusters mimic the interaction of the Mo edge and S edge with the surface.

The four above mentioned crystallographic surfaces of γ-alumina and anatase-TiO_2 were considered. In figures 5 and 6, the Gibbs free energy diagrams of the Mo_6S_n clusters supported on γ-Al_2O_3(110) and TiO_2(101) show that for high chemical potential of sulfur, $\Delta\mu_S$ (i.e. strong sulfiding conditions), the stable Mo_6S_{24} cluster is fully sulfided on both supports and is oriented in a parallel (‖) mode ('raft'-like mode), such as shown in figure 7(a) for the (110) γ-Al_2O_3 surface. Van der Waals and hydrogen bonding interactions are predominant between the sulfur atoms of the cluster and oxygen atoms and hydroxyls. The approximate treatment of van der Waals contributions was explained in [59, 60]. In a

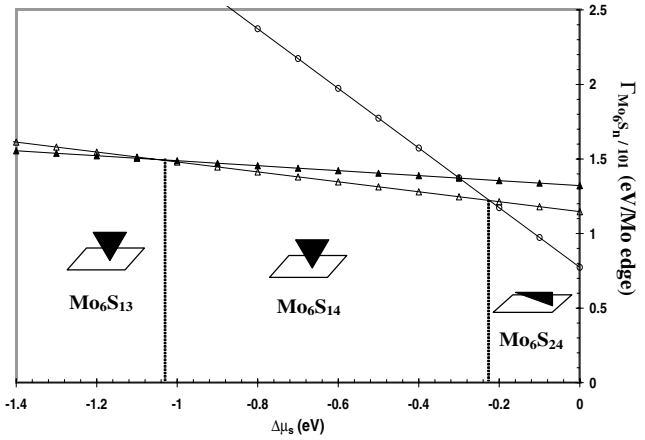

Figure 5. Gibbs free energy diagram of the Mo_6S_n clusters adsorbed on the γ-alumina (110) surface. ○, Mo_6S_{24} (∥); Δ, Mo_6S_{14} (⊥); ▲, Mo_6S_{13} (⊥). (Only the most stable configurations are represented, according to [59].) Reprinted from [59]. Copyright 2005, with permission from Elsevier.

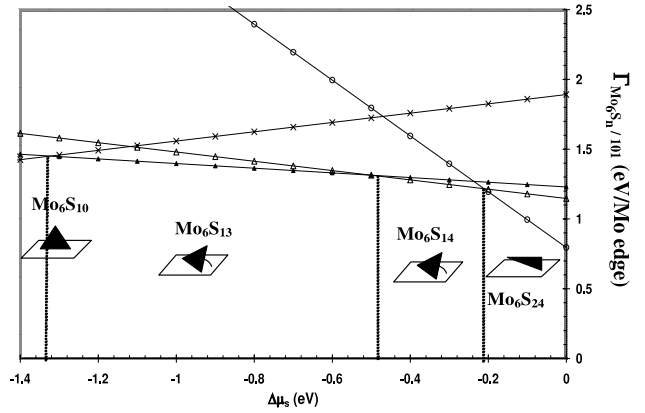

Figure 6. Gibbs free energy diagram of the Mo_6S_n clusters adsorbed on the anatase-TiO_2(101) surface. ○, Mo_6S_{24} (∥); Δ, Mo_6S_{14} (tilted); ▲, Mo_6S_{13} (tilted); ×, Mo_6S_{10} (⊥). (Only the most stable configurations are represented, according to [59].) Reprinted from [59]. Copyright 2005, with permission from Elsevier.

more reductive environment (lower value of $\Delta\mu_S$), Mo_6S_{14} or Mo_6S_{13} clusters are stabilized in a perpendicular (⊥) orientation with Mo–O–Al or Mo–O(S)–Ti chemical bonds (figures 7(b)–(d)). The DFT optimized Mo–O lengths (about 2.0 Å) are compatible with EXAFS distances reported in the literature [58].

The most striking result was observed for anatase-TiO_2, where there is an epitaxial relationship between the Mo edge of the Mo_6S_{14} or Mo_6S_{13} clusters and the surface oxygen and titanium atomic networks as visualized in figures 7(c) and (d). Even if this epitaxial relationship is not perfect due to a slight mismatch between Mo–Mo and Ti–Ti distances, the local epitaxial relationship involving finite edge lengths contributes to the stabilization of strongly interacting particles in a tilted configuration such as represented in figures 7(c) and (d). This behaviour observed for anatase-TiO_2 and not observed for γ-alumina is at the origin of the different wetting effects of the two supports by MoS_2 particles.

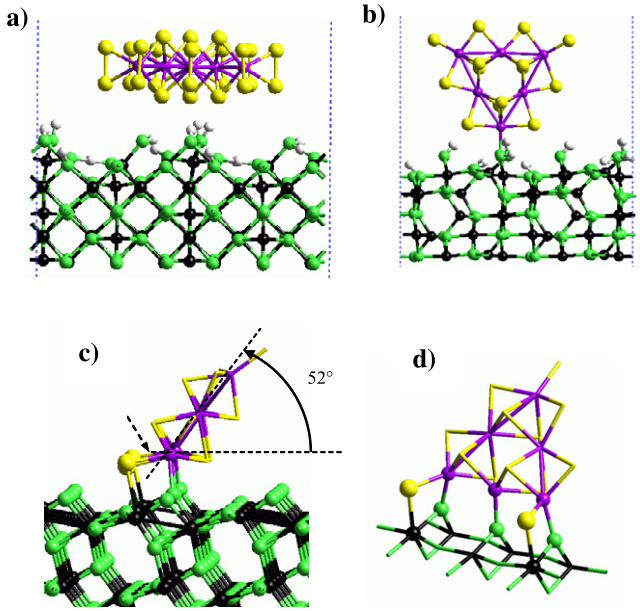

Figure 7. Optimized structures of (a) 'raft'-like Mo_6S_{24} cluster on the hydroxylated (110) γ-alumina surface, (b) perpendicular Mo_6S_{14} cluster on the hydroxylated (110) γ-alumina surface, (c) (respectively (d)) tilted Mo_6S_{14} (respectively Mo_6S_{13}) clusters on the (101) anatase-TiO_2 (with epitaxy). Yellow balls, sulfur; magenta balls, molybdenum; green balls, oxygen; white balls, hydrogen. (For interpretation of the references to color in this figure legend, the reader is referred to the web version of this article.) Reprinted from [59]. Copyright 2005, with permission from Elsevier.

Considering the data obtained on the S-edge and Mo-edge particles interacting with the supports, the determination of the shape of the MoS_2 nano-particles anchored on alumina or anatase at the thermodynamic equilibrium was obtained by using the Gibbs–Curie–Wulff–Kaischew (GCWK) approach [61, 62]. This approach is commonly used for supported metallic particles [63].

The two schematic representations in figure 8(a) depict the GCWK morphology of a particle anchored through the Mo edge (corresponding to the atomic structure in figure 7(b)) or lying in a parallel orientation to the support's surface (figure 7(a)). Using the schematic representations and notations of figures 8(a) and (b), the geometric parameters of the anchored particles can be deduced from the GCWK equations:

$$\frac{h_{Mo}}{\Gamma_{Mo}} = \frac{h_S}{\Gamma_S} = \frac{h_{Mo}^{anch}}{\Gamma_{Mo}^{anch}} \tag{3}$$

where h are the distances of the centre of the virtual non-interacting particle from the corresponding edges, Γ_{Mo} and Γ_S the surface energies of the free edges, and Γ_{Mo}^{anch} the surface energy of the anchored Mo edge (note $h_{Mo}^{anch} = h_{Mo} - \Delta h$).

According to this definition, h_{Mo}^{anch} and Γ_{Mo}^{anch} are algebraic values and are allowed to become negative, because h_{Mo}^{anch} is the centre height or depth of the virtual non-interacting particle. Γ_{Mo}^{anch} depends on the adhesion energies (negative by convention if anchoring through the Mo edge exists) and the chemical potential of S:

$$\Gamma_{Mo}^{anch}(\Delta\mu_S) = \Gamma_{Mo}(\Delta\mu_S) + E_{adh}. \tag{4}$$

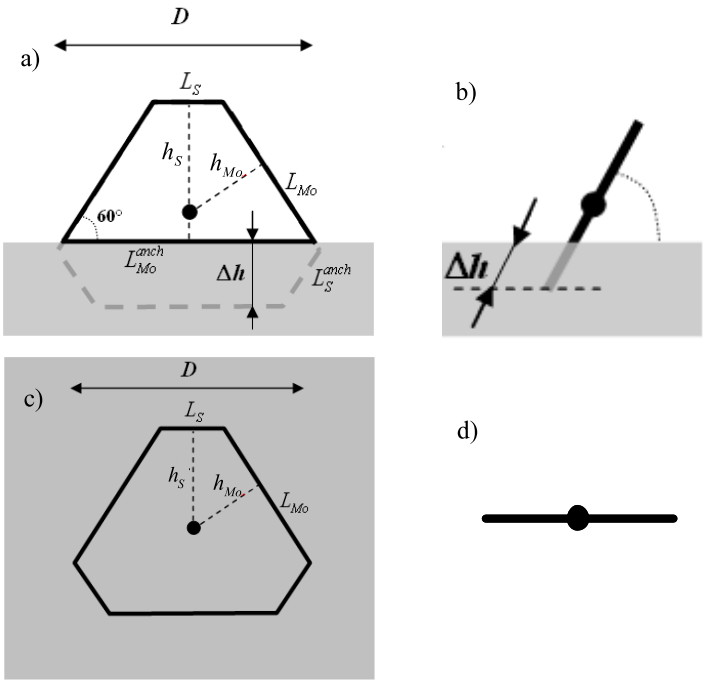

Figure 8. (a) Front and (b) side views of the MoS_2 particle with Mo-edge wetting (tilted orientation); (c) top and (d) side views of the MoS_2 particle with basal wetting (parallel orientation). Reprinted from [60]. Copyright 2007, with permission from Elsevier.

From equations (3) and (4) the following relationship results:

$$\frac{\Delta h}{h_{\mathrm{Mo}}} = \frac{-E_{\mathrm{adh}}}{\Gamma_{\mathrm{Mo}}} = 1 - \beta \tag{5}$$

where $\beta = \Gamma_{\mathrm{Mo}}^{\mathrm{anch}} / \Gamma_{\mathrm{Mo}}$ (according to the value of E_{adh}, $\beta = 0.19$). In the same spirit as for metallic particles [63], different edge wetting regimes of the supported MoS_2 particles can be defined as a function of the $\Delta h / h_{\mathrm{Mo}}$ ratio.

For $-1 < \beta < 1$, there is edge wetting by the Mo edge (figures 8(a) and (b)).

For $\beta \geqslant 1$, there is no edge wetting by the Mo edge: the particle lies parallel to the surface. This is defined as the basal wetting of the support by the particles (figures 8(c) and (d)).

For $\beta \leqslant -1$, the edge wetting is perfect.

The other relevant geometric parameters ($\frac{L_{\mathrm{Mo}}^{\mathrm{anch}}}{L_{\mathrm{Mo}}}$, $\frac{L_{\mathrm{S}}^{\mathrm{anch}}}{L_{\mathrm{S}}}$, $\frac{L_{\mathrm{S}}}{L_{\mathrm{Mo}}}$) for the morphology can be expressed as a function of β and $\alpha = \Gamma_{\mathrm{S}} / \Gamma_{\mathrm{Mo}}$.

It was found by DFT calculations that unsupported (isolated) MoS_2 particles ($E_{\mathrm{adh}} = 0$ or $\beta \geqslant 1$) have a deformed hexagonal shape exposing more Mo edge than S edge ($\alpha = 1.35$), due to the lower surface energy of the Mo edge [64, 65]. We expect that depending on the interaction with the support ($E_{\mathrm{adh}} \neq 0$) the equilibrium morphology changes. According to [59, 60], anatase-TiO_2 supported MoS_2 particles exhibit a $\Delta h / h_{\mathrm{Mo}}$ ratio smaller than unity ($\beta = 0.19$), which characterizes the 'edge wetting regime' of the sulfide particles anchored through the Mo edge for diameter smaller than 45 Å. Beyond this size, van der Waals interactions are predominant and flat lying particles (with basal wetting) are favoured. The morphology of anatase supported MoS_2 particles can be defined as trapezoidal for diameter smaller than 45 Å as shown in the schematic representation of figures 8(a) and (b). In contrast, for γ-alumina supported MoS_2 particles the adhesion energies are too weak, and most of the MoS_2 particles lie in a parallel orientation (basal wetting) with a deformed hexagonal shape whatever the size (figures 8(c) and (d)).

Considering these morphologies for anchored and non-anchored particles, the proportion of edge sites (anchored, non-anchored, S edge and Mo edge) is deduced from particle diameter as reported in figures 9 and 10. The average MoS_2 particle size calculated from TEM histograms reported in [54] is around 38 Å for the titania support and it is around 49 Å for γ-alumina. Using these two diameter values in the diagrams of figure 9 leads to a similar proportion of free edge sites (including non-anchored Mo- and S edges) on anatase-TiO_2 (25–30%) and γ-alumina (24–29%). The number of Mo-edge atoms trapped at the MoS_2/anatase interface is thus compensated by the smaller sizes of edge anchored particles and the decrease of Mo bulk atoms. Hence, the calculated proportion of free edge sites cannot explain the different intrinsic HDS activity (expressed by Mo atom) observed on anatase and alumina. According to figure 10, the relative distribution of S-edge and Mo-edge sites is 21% on anatase and 38% on γ-alumina for the two sizes. The loss of two S edges on anatase is induced by the edge wetting of anatase. Furthermore, Arrouvel *et al* [59] found that anatase anchored MoS_2 clusters stabilize sulfur deficient particles, exhibiting more vacancies, required for the HDS reaction. These two combined effects certainly elucidate the enhancement of the intrinsic activity on anatase-TiO_2 as observed in [54] for non-promoted particles. As a consequence, the higher intrinsic HDS activity observed on anatase is explained by the different nature of edge sites exposed by the supported MoS_2 particles.

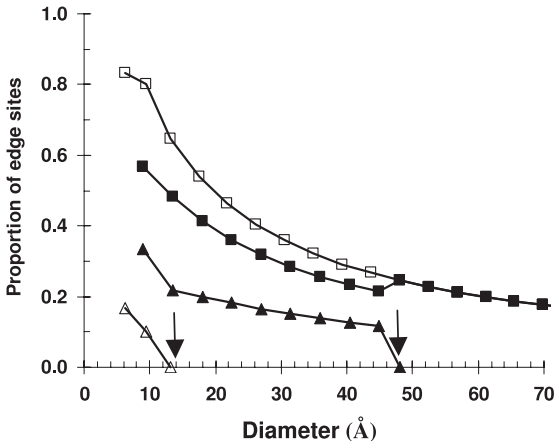

Figure 9. Proportion of non-anchored (free) and anchored Mo-edge sites (with respect to the total number of Mo atoms) as a function of the MoS_2 particle diameter. Δ, Mo-edge atoms anchored on γ-alumina (L_{Mo}^{anch}); □, free Mo sites at S and Mo edge on γ-alumina; ▲, Mo-edge atoms anchored on anatase; ■, free Mo sites at the S and Mo edge on anatase. Arrows represent the size transition between edge-anchored (edge-wetting) particles and flat lying particles (basal wetting). Reprinted from [60]. Copyright 2007, with permission from Elsevier.

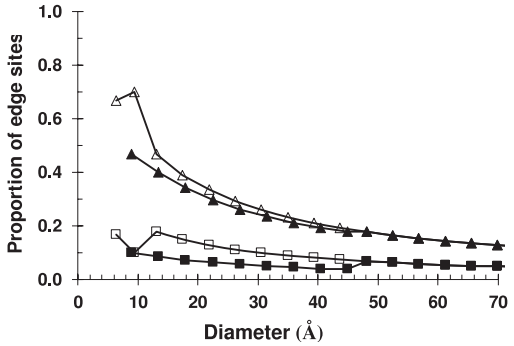

Figure 10. Distribution of free edge sites: Δ, Mo-edge sites on γ-alumina; □, S-edge sites on γ-alumina; ▲, Mo-edge sites on anatase; ■, S-edge sites on anatase. Reprinted from [60]. Copyright 2007, with permission from Elsevier.

5. Effects of hydroxylation of the γ-alumina surface on the properties of Pd particles

As shown in section 3, the hydroxyl coverage of the relevant (100) and (110) surfaces of γ-Al_2O_3 depends on temperature and water pressure [28, 45]. During the preparation steps of the catalysts and the hydrogenation reactions, the supported γ-alumina Pd material is usually exposed to temperatures in the 473–573 K range [12]. Furthermore, scanning tunnel microscopy (STM) studies on Rh particles supported on an alumina thin film revealed how the nucleation and dispersion of metal particles may change with the hydroxylation of the film [66, 67]. Hence, the hydroxylation state of the support appears as an important parameter influencing the active phase behaviour.

In what follows, we report three relevant examples extracted from the work by Valero *et al* [68–71] and illustrating how DFT calculations helped to investigate the effect of hydroxylation of γ-alumina surfaces on their interaction with Pd particles.

The first interesting result reported in [69] concerns the effect of hydration of the γ-alumina (110) surface on the potential energy surface (PES) of one Pd atom. The dehydrated surface is extremely corrugated and the presence of unsaturated aluminium atoms makes this surface very reactive. As explained in section 3, the surface is hydrated even after a treatment at high temperature (up to 1100 K). According to [28, 45], this surface contains 5.9 H_2O nm^{-2} at 600 K and normal water pressure (figure 1(c)).

The computed potential energy surfaces (PES) of the Pd atom on the dehydrated and hydrated γ-Al_2O_3(110) surfaces are shown in figures 11(a) and (b) respectively. Adsorption energies for the dehydrated surface vary from −1.0 to −1.8 eV (figure 11(a)). The strongest binding site is in the vicinity of the Al_{III} site, which exhibits the highest unsaturation. On the other hand, adsorption energies are overall reduced for the hydrated γ-Al_2O_3 surface and vary from −0.2 to −1.6 eV (figure 11(b)), although the optimum adsorption situation is only slightly destabilized. The dissociative adsorption of water decreases the Lewis acidity of the Al surface atoms and the Lewis basicity of the O surface atoms. The stable adsorption site of Pd on the dehydrated surface compared to the non hydrated surface is completely changed since the Al site is saturated by an OH group, while the vicinal oxygen atoms are bearing a proton. The strongest binding site for the hydrated surface exhibits multiple bonds between palladium and two μ_1-OH sites, one Al_V aluminium and a weak interaction with a proton of the μ_3-OH group. When trapped in this specific hydroxyl environment, the Pd adsorption energy remains large

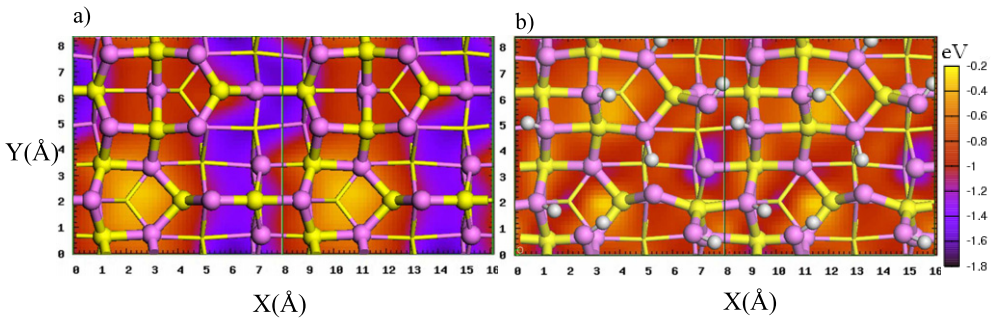

Figure 11. (2 × 1) view of the potential energy surface (PES) of the palladium atom on the (110) surface of γ-alumina: (a) dehydrated; (b) hydrated. Violet balls, O; yellow balls, Al; white balls, H. (For interpretation of the references to color in this figure legend, the reader is referred to the web version of this article.) Reprinted with permission from [69]. Copyright 2006 American Physical Society.

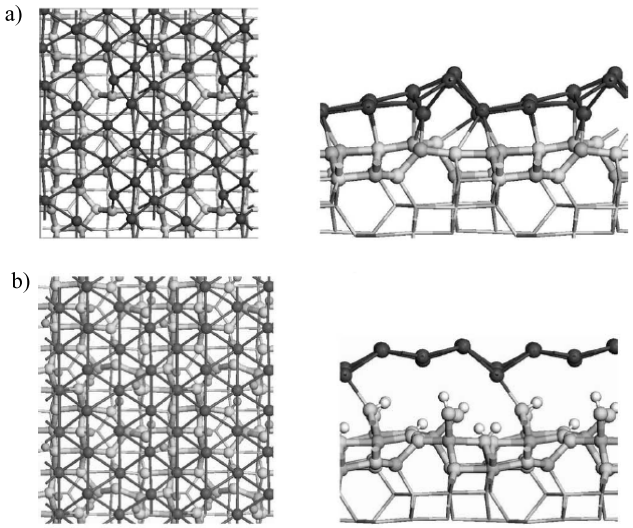

Figure 12. Strained Pd(111) films on the γ-alumina surfaces: (a) non-hydrated (110) surface (top and side views), (b) hydrated (110) surfaces (top and side views). Reprinted figure with permission from [70]. Copyright 2007 American Physical Society.

(−1.6 eV); however, it decreases quickly for other positions on the surface, in contrast with the dehydrated surface, where the sticking is high on a very large fraction of the surface. Subsequent consequences for the diffusion properties of Pd atoms on the surfaces have been proposed in [69].

If we now consider the adsorption of a Pd(111) film on the same type of surfaces (figure 12), the wetting properties of the Pd film were found to depend also on the hydroxylation state of the surface [70]. To evaluate the wetting properties, a Young–Dupré approach was considered and the work of adhesion of the Pd film was calculated. The wetting regime and the morphology of the Pd particles can thus be deduced (in a similar way as presented in section 4 for MoS_2 particles). Figures 12(a) and (b) reveal the effect of the surface hydroxylation on the local structure of the film after adsorption. The resulting work of adhesion is decreased from 0.89 J m^{-2} for the non-hydrated (110) surface to 0.20 J m^{-2} for the hydrated surface. This is in line with the above mentioned result on the adsorption of single Pd atoms on the same surfaces, where the average metal–support interaction was significantly weaker on the hydrated surface. According to estimated values of the wetting parameter ($0 < \beta < 1$), the wetting of the support by Pd particles is weak for all surfaces and the shape of the supported Pd particles is mainly 3D.

The last example concerns the influence of the type of support surface on the adsorption mode of small molecules on Pd_4 clusters. In our recent study [71], it was shown that the interplay between molecular adsorption and metal–support interaction for γ-alumina supported Pd clusters plays a role in the adsorption of small molecules such as CO and C_2H_4 on Pd_4 clusters. In order to optimize the Pd_4–molecule and the Pd_4–alumina interaction, the Pd_4 cluster and, locally, the substrate deforms spontaneously, storing a substantial strain energy. In particular for the CO molecule, the calculations have revealed that Pd_4–CO interactions are strongly counterbalanced by the contribution of substrate deformation energy. In the case of C_2H_4, substrate deformation energies are smaller, although they cannot be neglected. The adsorption of CO molecules induces a weakening of the cluster Pd–Pd bonds and a strengthening of the interaction between Pd atoms and surface sites. Moreover, a strong trans effect between the surface O electron donor groups and the electron acceptor CO molecule was found for the η_2 and η_3 adsorption modes. This results in a counter-intuitive increase of cluster–oxide interaction upon CO adsorption. In contrast, the adsorption of ethylene molecules, with a stronger electron donor character, cannot present such a synergy in electron transfer with the surface, especially for the π mode. As a result, the metal–support interaction is weakened upon ethylene adsorption.

The two γ-Al_2O_3 surfaces behave differently upon adsorption of an incoming ligand. Indeed, Pd–ligand interactions affect electronic states at the Pd_4/γ-$Al_2O_3(100)$ interface, whereas the Pd_4/γ-$Al_2O_3(110)$ interface is less perturbed by the presence of an adsorbate. The stability of CO adsorbed molecules increases in the order $\eta_1 < \eta_2 < \eta_3$ for isolated Pd_4 and supported Pd_4 clusters (whatever the support's surface). However, as shown in figure 13, the adsorption mode of C_2H_4 switches from the π mode on isolated Pd_4 and Pd_4/γ-$Al_2O_3(110)$ clusters to the di-σ mode on Pd_4/γ-$Al_2O_3(100)$. The adsorption of ethylene molecules, with a stronger electron donor character and a delicate interplay between the energy position of π and π^* orbitals, makes the trend of C_2H_4 adsorption more sensitive to the substrate's hydroxylation state. This result may offer new insights into the effects of hydroxylation on the hydrogenation activity of olefins in the case of highly dispersed metal particles.

6. Conclusions

We have reported recent results obtained by DFT simulations on the influence of support–active phase interaction for industrially used catalytic materials: γ-alumina and anatase-TiO_2 supported MoS_2 catalysts and γ-alumina supported Pd catalysts. *First principles* surface thermodynamics simulations at equilibrium have thus brought relevant insights for surfaces and interfaces at an atomistic scale coherent with various experimental characterizations (IR, NMR) and this approach may also go beyond some experimental limitations. The results obtained so far may also serve as the basis for the study of more complex 'out of equilibrium' processes by using first principles kinetic Monte Carlo as recently proposed for oxidation catalysis [72].

General concepts such as the dependence of wetting properties on the nature of the oxide surface have been put forward. For MoS_2 catalysts, the morphology of the supported particles can be significantly modified by the epitaxy relationship between one edge of the MoS_2 nano-sheets and the anatase-TiO_2 surfaces. To a certain extent, this concept can be compared to dye–anatase systems, where the dye ordering on the anatase surface depends on the local structure of the surface atomic lattice, which modifies the spectral response [2]. For anatase supported MoS_2 catalysts, the anchorage mode

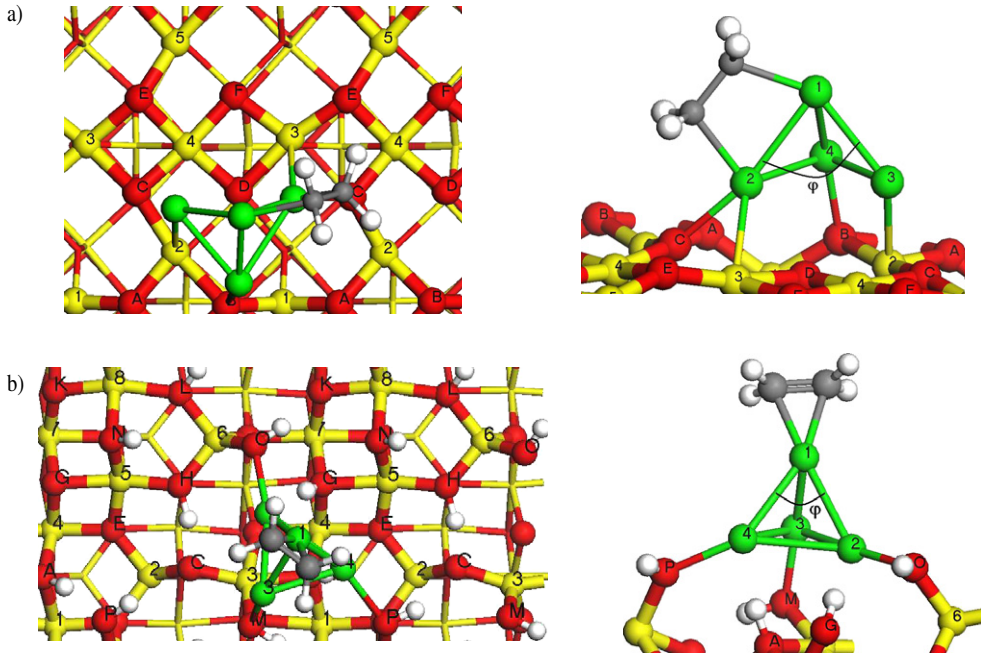

Figure 13. Top views (left) and side views (right) of the most stable configurations of C_2H_4 adsorbed on the Al_2O_3 supported Pd_4 clusters: (a) (100) surface and (b) (110) surface (yellow balls, Al; red balls, O; green balls, Pd; small white balls, H; grey balls, C). (For interpretation of the references to color in this figure legend, the reader is referred to the web version of this article.) Reprinted from [71]. Copyright 2007, with permission from Elsevier.

of the active phase on the local surface sites influences the resulting catalytic activity. Pushing further the analogy between the two systems also reveals that epitaxy relationships on the anatase (101) surface can be found either for specific dye molecules [2], or for the MoS_2 active phase [59]. In the case of γ-alumina supported Pd materials, the role of hydroxylation is crucial at different levels. In a similar way as for MoS_2 catalysts, the wetting by Pd particles of the support competes with the wetting by water molecules. Finally, one striking result is that the adsorption mode of an olefin on a Pd_4 cluster also depends on the hydroxylation state of the alumina surface. This result may have significant consequences for the hydrogenation activity and will be further investigated in future works.

Acknowledgments

P Raybaud addresses a special thanks to Michèle Breysse from Université Pierre et Marie Curie for her very fruitful collaboration within the experimental field of supported sulfide catalysts.

References

[1] Euzen P, Raybaud P, Krokidis X, Toulhoat H, Loarer J-L L, Jolivet J-P and Froidefond C 2002 *Handbook of Porous Solids* vol 3 (Weinheim: Wiley–VCH)
[2] Ushiroda S, Ruzycki N, Lu Y, Spitler M T and Parkinson B A 2005 *J. Am. Chem. Soc.* **127** 5158
[3] Wang H, Wu Y and Xu B-Q 2005 *Appl. Catal.* B **59** 139
[4] Breysse M, Portefaix J L and Vrinat M 1991 *Catal. Today* **10** 489
[5] Topsøe H, Clausen B S and Massoth F E 1996 *Hydrotreating Catalysis—Science and Technology* vol 11 (Berlin: Springer)
[6] Prins R 1997 *Handbook of Heterogeneous Catalysis* vol 4 (Weinheim: Wiley–VCH)
[7] Raybaud P, Hafner J, Kresse G and Toulhoat H 1997 *J. Phys. Condens. Matter.* **9** 11085
[8] Raybaud P, Hafner J, Kresse G and Toulhoat H 1997 *J. Phys. Condens. Matter.* **9** 11107
[9] Rohrbach A, Hafner J and Kresse G 2003 *J. Phys. Condens. Matter* **15** 979
[10] Raybaud P 2007 *Appl. Catal.* A **322** 76
[11] Argo A M, Odzak J F, Lai F S and Gates B C 2002 *Nature* **415** 623
[12] Benkhaled M, Morin S, Pichon C, Thomazeau C, Verdon C and Uzio D 2006 *Appl. Catal.* A **312** 1
[13] Henry C R 1998 *Surf. Sci. Rep.* **31** 231
[14] Hohenberg P and Kohn W 1964 *Phys. Rev.* B **136** 864
[15] Kohn W and Sham L J 1965 *Phys. Rev.* A **140** 1133
[16] Kresse G and Furthmüller J 1996 *Comput. Mater. Sci.* **6** 15
[17] http://cms.mpi.univie.ac.at/vasp
[18] http://www.camp.dtu.dk/campos
[19] http://www.wien2k.at
[20] Payne M C, Teter M P, Allan D C, Arias T A and Joannopoulos J D 1992 *Rev. Mod. Phys.* **64** 1045
[21] Scheffler M and Dabrowski J 1988 *Phil. Mag.* A **58** 107
[22] Quian G X, Martin R M and Chadi D J 1988 *Phys. Rev.* B **38** 7649
[23] Kadas K, Kern G and Hafner J 1998 *Phys. Rev.* B **58** 1
[24] Wang X-G, Weiss W, Shaikhutdinov S K, Ritter M, Petersen M, Wagner F, Schlögl R and Scheffler M 1999 *Phys. Rev. Lett.* **81** 1038
[25] Reuter K, Stampfl C and Scheffler M 2005 *Handbook of Materials Modeling—Ab initio Thermodynamics and Statistical Mechanics of Surface Properties and Functions* vol 1 (Berlin: Springer)
[26] Raybaud P, Hafner J, Kresse G, Kasztelan S and Toulhoat H 2000 *J. Catal.* **189** 129

[27] Raybaud P, Hafner J, Kresse G, Kasztelan S and Toulhoat H 2000 *J. Catal.* **190** 128
[28] Digne M, Sautet P, Raybaud P, Euzen P and Toulhoat H 2002 *J. Catal.* **211** 1
[29] Perdew J P and Wang Y 1992 *Phys. Rev.* B **45** 13244
[30] Vanderbilt D 1990 *Phys. Rev.* B **41** 7892
[31] Kresse G and Hafner J 1994 *Phys. Rev.* B **49** 14251
[32] Kresse G and Joubert D 1999 *Phys. Rev.* B **59** 1758
[33] Lippens B C and Boer J H d 1964 *Acta Crystallogr.* **17** 1312
[34] Hietala J, Root A and Knuuttila P 1994 *J. Catal.* **150** 46
[35] Canio E C D, Edwards J C and Bruno J W 1994 *J. Catal.* **148** 76
[36] Guillaume D, Gautier S, Alario F and Devès J M 1997 *Oil Gas Sci. Technol.-Rev. IFP* **54** 537
[37] Tsyganenko A A and Filimonov V N 1973 *J. Mol. Struct.* **19** 579
[38] Knözinger H and Ratnasamy P 1978 *Catal. Rev. Sci. Eng.* **17** 31
[39] Morterra C and Magnacca G 1996 *Catal. Today* **27** 497
[40] Saad A B M, Ivano V A, Lavalley J C, Nortier P and Luck F 1993 *Appl. Catal.* **94** 71
[41] Nortier P, Fourre P, Saad A B M, Saur O and Lavalley J-C 1990 *Appl. Catal.* **61** 141
[42] Krokidis X, Raybaud P, Gobichon A-E, Rebours B, Euzen P and Toulhoat H 2001 *J. Phys. Chem.* B **105** 5121
[43] Wolverton C and Haas K C 2001 *Phys. Rev.* B **63** 024102
[44] Paglia G, Rohl A L, Buckley C E and Gale J D 2005 *Phys. Rev.* B **71** 224115
[45] Digne M, Sautet P, Raybaud P, Euzen P and Toulhoat H 2004 *J. Catal.* **226** 54
[46] Arrouvel C, Digne M, Breysse M, Toulhoat H and Raybaud P 2004 *J. Catal.* **222** 152
[47] Arrouvel C, Breysse M, Toulhoat H and Raybaud P 2004 *J. Catal.* **226** 260
[48] Morterra C, Ghiotti G, Bocuzzi F and Coluccia S 1978 *J. Catal.* **51** 299
[49] Busca G, Lorenzelli V, Escribano V S and Guidetti R 1991 *J. Catal.* **131** 167
[50] Travert A, Manoilova O V, Tsyganenko A A, Maugé F and Lavalley J C 2002 *J. Phys. Chem.* B **106** 1350
[51] Dzwigaj S, Arrouvel C, Breysse M, Geantet C, Inoue S, Toulhoat H and Raybaud P 2005 *J. Catal.* **236** 245
[52] Coulier L, van Veen J A R and Niemantsverdriet J W 2002 *Catal. Lett.* **79** 149
[53] Breysse M, Afanasiev P, Geantet C and Vrinat M 2003 *Catal. Today* **86** 5
[54] Ramirez J, Fuentes S, Díaz G, Vrinat M, Breysse M and Lacroix M 1989 *Appl. Catal.* **52** 211
[55] Shimada H 2003 *Catal. Today* **86** 17
[56] Ramirez J, Cedeno L and Busca G 1999 *J. Catal.* **184** 59
[57] Wang D, Qian W, Ishihara A and Kabe T 2002 *Appl. Catal.* A **224** 191
[58] Leliveld R G, van Dillen A J, Geus J W and Koningsberger D C 1997 *J. Catal.* **165** 184
[59] Arrouvel C, Breysse M, Toulhoat H and Raybaud P 2005 *J. Catal.* **232** 161
[60] Costa D, Arrouvel C, Breysse M, Toulhoat H and Raybaud P 2007 *J. Catal.* **246** 325
[61] Curie M P 1885 *Bull. Soc. Min. France* **8** 145
[62] Wulff G 1901 *Z. Kristallogr.* **34** 449
[63] Henry C R 2005 *Prog. Surf. Sci.* **80** 92
[64] Schweiger H, Raybaud P, Kresse G and Toulhoat H 2002 *J. Catal.* **207** 76
[65] Lauritsen J V, Nyberg M, Nørskov J K, Clausen B S, Topsøe H, Lægsgaard E and Besenbacher F 2004 *J. Catal.* **224** 94
[66] Heemeier M, Frank M, Libuda J, Wolter K, Kuhlenbeck H, Bäumer M and Freund H J 2000 *Catal. Lett.* **68** 19
[67] Libuda J, Frank M, Sandell A, Andersson S, Bruhwiler P A, Bäumer M, Martensson N and Freund H J 1997 *Surf. Sci.* **384** 106
[68] Valero M C, Digne M, Sautet P and Raybaud P 2006 *Oil Gas Sci. Technol. Rev. IFP* **61** 535
[69] Valero M C, Raybaud P and Sautet P 2006 *J. Phys. Chem.* B **110** 1759
[70] Valero M C, Raybaud P and Sautet P 2007 *Phys. Rev.* B **75** 045427
[71] Valero M C, Raybaud P and Sautet P 2007 *J. Catal.* **247** 339
[72] Reuter K, Frenkel D and Scheffler M 2004 *Phys. Rev. Lett.* **93** 116105